Assessing the effects of link-repair sequences on road network resilience

Philippe Y.R. Sohouenou[1] and Luis A.C. Neves[2]

[1,2]Resilience Engineering Research Group, Faculty of Engineering, The University of Nottingham, Nottingham, UK

[1]Nottingham Transportation Engineering Centre, Faculty of Engineering, The University of Nottingham, Nottingham, UK

[1]Email: evxps12@nottingham.ac.uk

June 27, 2021

Abstract

Disruptions to transport networks are inevitable and detrimental to the functioning of society. Improving the resilience of transport networks to disruptive events has, therefore, a significant impact on society. Although the resilience of a transport system depends on the ability of the network to sustain the consequences of initial disruption (i.e. robustness) and quickly recover its performance (i.e. rapidity), the latter attracted less attention than robustness. The present paper focuses on quantifying the impacts of recovery processes and, more specifically, link-repair strategies on resilience. Several link-repair strategies are compared across a multitude of perturbation scenarios in the well-known Sioux Falls network. The strategies considered include: (i) the optimal (minimising the disruption consequences over the recovery process), (ii) average (representing a recovery process where the disrupted links are repaired in random order), (iii) flow-based (where the links with the highest traffic flow in the undisrupted network are repaired first), and (iv) criticality-based (where the links whose individual failure result in the highest impacts on the system performance are repaired first) recovery. The results of this comparison are subsequently used to evaluate the correlation between robustness and resilience, and characterise the optimal repair strategy.

Keywords: Resilience assessment, Network robustness, Recovery, Link-repair process, Road networks, Link criticality, Traffic congestion

In print, color should be used for: Figures 1, 3, 4, 5, 6 and 7.

Nomenclature

τ	Time elapsed since the start of the recovery
a	A link in a road network
c_a	Capacity of link a
d_w	Travel demand on the OD pair w
k_w	Weighting factor associated with the OD pair w
N_H	Maximum number of links that can be repaired between t_0 and t_H
NP	Road network performance indicator
RE	Road network resilience indicator
RO	Road network robustness indicator
t	Time
t_0	Start time of the recovery process
t_H	Time horizon chosen to compute RE
TT	Travel Time
TT_0^w	Undisrupted TT along w
tt_a	Travel time of link a
tt_a^f	Free-flow travel time of link a
TT_d^w	Disrupted TT along w
TTC_w	TT relative change index - along w
USD	Proportion of unsatisfied demand
w	Origin-Destination (OD) pair
x_a	Flow on link a
2LF	Two-link failure

3LF	Three-link failure
4LF	Four-link failure
BPR	Bureau of Public Roads
FW	Franke-Wolfe (algorithm)
MLF	Multiple-link failure
OD	Origin-Destination
SLF	Single-link failure

1 Introduction

1.1 Background

Disruptions to transport networks are inevitable and detrimental to the functioning of society. Road disruptions directly affect users through greater congestion, loss of time, and higher fuel consumption, but also lead to indirect impacts, including constrained access to jobs and services as well as poorer air quality (Hallegatte et al., 2019). The impacts on businesses include sales losses, delays in supply and delivery as well as diminished competitiveness in international markets (Hallegatte et al., 2019). For instance, Pelling et al. (2002) estimated that the 1995 earthquake in Kobe (Japan) increased the regional transportation costs and cost of goods by over 50% and 10%, respectively. Xie and Levinson (2011) estimated that the collapse of the I-35W Bridge in Minneapolis (USA) resulted in economic losses of US$71,000 to US$220,000 a day. Hence, it is now recognised that society would benefit from resilient road networks (i.e. able to sustain, resist and rapidly recover from disruptions) and, as such, the interest on methods that allow the quantification and optimisation of road network resilience has increased recently (Bhavathrathan and Patil, 2018; Ganin et al., 2017; Martinson, 2017).

Resilient systems are associated with several properties, including robustness—the ability to resist and absorb perturbations—and rapidity (or recoverability)—the ability to recover quickly. Several generic (i.e. applicable to any system using the appropriate context-specific functions) frameworks were developed to assess the resilience of engineering systems. These frameworks include the seminal work of Bruneau et al. (2003) that defines robustness and rapidity as the key measures that should be used to quantify resilience and introduces a graphical interpretation of the resilience concept where the latter is measured by the integral of the quality of infrastructure over time. Henry and Ramirez-Marquez (2012) propose a time-dependent-system-resilience measure

alongside with a time-to-recover- and a resilience-cost metric. More recently, Sharma et al. (2018) proposed a series of partial descriptors based on the analogy of the system recovery curve with a cumulative distribution function in probability theory including resilience "centre" and skewness. Alternatively, context-specific resilience frameworks were developed for various types of critical networked infrastructures such as control systems (Alcaraz, 2018), smart grids (Alcaraz et al., 2018) and intermodal freight networks (Chen and Miller-Hooks, 2012).

In the context of road networks, most works (Bhavathrathan and Patil, 2018; Ganin et al., 2017; Gauthier et al., 2018; Omer et al., 2013) focus on robustness while rapidity has attracted less attention. Still, considering the socio-economic consequences of road disruptions, recovery processes can have an important influence on the welfare of society as they can help alleviate disruption consequences in the early stage recovery. The studies that consider recovery processes propose different approaches. Nogal et al. (2016) and Nogal and Honfi (2019) focus on the gradual adaptation of road users following both the perturbation and restoration phases. Tuzun Aksu and Ozdamar (2014) develop a model optimising the link-repair sequence to quickly recover the network connectivity to facilitate evacuations. Zhang et al. (2017) develop a model optimising the link-repair sequence to quickly improve the network performance under stochastic damage levels and repair durations. Finally, Hu et al. (2016), compare different repair strategies under random (damaging random sets of links), localised (damaging adjacent links), and malicious (seeking to maximise the damage to the system performance) perturbations. However, the studies of Hu et al. (2016), Tuzun Aksu and Ozdamar (2014) and Zhang et al. (2017) rely on topological network models and performance metrics that do not consider link capacity constraints. This approach can significantly overestimate the resilience of road networks, particularly when analysing congested networks.

Ultimately, although research has contributed to the understanding of road network robustness and resilience, understanding of the role of rapidity and therefore recovery strategies in the resilience of congested road networks is still limited. To increase this understanding, the present paper compares the performance of several recovery strategies across a full range of disruption scenarios in the Sioux Falls network (LeBlanc et al., 1975). To this end, a traffic model accounting for capacity constraints and congestion is adopted. The analysis is performed on the Sioux Falls network for two reasons. The first reason is computational effectiveness. This network model is composed of 24 nodes and 76 directed links, leading to reasonable traffic-simulation run times (under five seconds). This short computational time allowed the performance of over 80,000 disruption and repair simulations using parallel processing on a standard computer. The second reason is reproducibility. The Sioux Falls network dataset is readily available, for example, on the Transportation Networks for Research repository (Transportation Networks for Research Core

Team, 2019), and has been extensively used in the transport literature (Bhavathrathan and Patil, 2015; Mitradjieva and Lindberg, 2013; Wang et al., 2016).

1.2 Purpose, scope and structure of the paper

The present paper has two objectives: (i) evaluate how recovery strategies can help reduce disruption consequences, and (ii) characterise the optimal recovery strategy. To this end, this paper develops a road network resilience assessment framework suitable to model both the network robustness and rapidity under a full range of disruption scenarios.

In the traffic context, network resilience mainly depends on the consequences of the initial disruption to the network performance, the immediate response (in terms of closing lanes or reducing speed limits on affected roads) and the speed of restoring full functionality (through repair actions). As the present paper seeks to analyse and compare the performance of different repair strategies under a full range of potential disruption scenarios, the immediate response is considered outside the scope of this study. The recovery model focuses on the common element to all network recovery processes: the link repair sequence and its impact on the network performance. In reality, recovery processes could take many forms and durations depending on the nature of the disruption (car accident versus snow versus earthquake) and the resources allocated to response and repair. As detailed case-by-case modelling (Misra et al., 2020; Mitoulis et al., 2021) would be required to address this, the general framework presented here cannot take these into account and focuses instead on comparing link repair sequences without considering the duration of the repair actions performed on the individual links.

The study considers a full range of predictable and unpredictable disruption scenarios using the hazard-independent disruption model proposed in Sohouenou et al. (2021). All scenarios concurrently disrupting up to four links in the Sioux Falls network are modelled and classified into damage type (localised, random and targeted) and damage extension (single-, two-, three- and four-link failures) groups. The study then considers all possible link-repair sequences that can be implemented under each disruption scenario. This data is summarised into four recovery models. Firstly, the optimal (minimising the disruption consequences over the recovery process) and average (representing a basic recovery process where the disrupted links are repaired in random order) recovery curves are considered. These recovery models are compared and used to evaluate the variations in network resilience due to the network recovery strategy. To better characterise the optimal recovery strategy, two additional recovery models are considered and compared with the optimal recovery: the flow-based (where the links with the highest traffic flow in the undisrupted network are repaired first), and criticality-based (where the links whose individual failure would result in the highest impacts on the system performance are repaired first) recovery strategies.

The paper is structured as follows. Section 2 presents the methods and case study. In Sections 3 and 4, the results of the network resilience assessment are presented and discussed, respectively. Sections 5 provides some concluding remarks.

2 Methods

In this paper, the resilience assessment is divided into two main models: the disruption model (Section 2.1) and the recovery and resilience quantification model (Section 2.2), which are then applied to the case study (Section 2.3).

2.1 Disruption model and network performance quantification

2.1.1 Disruption model

Disruptive events can impact both the supply (i.e. the network) and the demand side (i.e. the flow of users) of the transport system. The supply side is affected by the damage induced on the infrastructures, which in turn impacts traffic conditions through road unavailability as well as speed and capacity reductions. The demand side can also be impacted as trips may be cancelled or delayed due to routes and destinations being affected. As this paper focusses on the impacts caused by variations in the supply side, travel demand was considered fixed (or independent of the network state) to effectively compare the network performance under different disruption scenarios (all other things being equal).

This research adopted an "all-hazard" approach (Sohouenou et al., 2021) that consists in simulating all possible combinations of link failures concurrently disrupting up to four links. These scenarios were then categorised into four damage extension (from single- to four-link failures) and three damage types (localised-, targeted-, and random-link failures).

It is noted that localised disruptions are normally specified in terms of hazard-prone areas derived from climate models (Casali and Heinimann, 2019; Demirel et al., 2015; Hu et al., 2016; Wisetjindawat et al., 2017). In this model, localised failures refer to a range of events that may differ in nature (flooding, landslide, or large demonstrations) but lead to similar consequences, that is, the unavailability of adjacent network components. They can be identified using the following procedure:

1. Identification of all localised two-link combinations

   (i) for each link, a_1, in the network, search for all links, $a_2 \neq a_1$, adjacent to a_1 (i.e. connected to the same node) and store (a_1, a_2) in a dataset

   (ii) remove duplicates from the dataset

2. Identification of all localised three-link combinations

   (i) for each link combination, (a_1, a_2), search for all links, $a_3 \neq a_1 \,\&\, a_2$, adjacent to a_1 and for all links, $a_3 \neq a_1 \,\&\, a_2$, adjacent to a_2, and store (a_1, a_2, a_3) in a dataset

   (ii) remove duplicates from the dataset

3. Identification of all localised four-link combinations

   (i) repeat step 2 using the localised three-link combination dataset

Unlike localised disruptions that lead to aggregated destruction of components in a limited area, targeted and random link failures can damage network components distributed throughout the whole system. The latter damage a random set of links (e.g. pavement maintenance, pipe bursting, or police incidents amongst others can lead to random road closures) whereas targeted attacks imply a driving force seeking to maximise damage to the network performance (e.g. the bombing of a critical bridge). In this model, targeted attacks correspond to the 5% scenarios in each damage extension group (dataset) that cause the highest increases in travel time, measured by the network robustness indicator (presented below, Eq. 3). The random failures correspond to the scenarios that are neither localised nor targeted.

The definitions, models and real-word events associated with these three types of events are described in Table 1. Sohouenou et al. (2021) show that random and localised disruptions generally lead to similar consequences while intentional attacks target links that may be apart or not critical on their own but whose combined disruptions create a maximised and widespread impact.

Table 1: Classification and model of disruptive events affecting road networks

Name	Definition	Model	Real-word events represented
Localised	Failure of adjacent links	Failures identified by the iterative procedure (above)	Flooding, Landslides, Large demonstrations
Targeted	Failure with a maximum impact on network performance	Failures leading to the bottom 5% robustness indicator values	Targeted bombing, Sabotage, Industrial actions
Random	Failure of randomly selected links in the network	Failures that are neither critical nor localised	Serious car accidents, Road works, Police incidents

2.1.2 Network performance quantification

As the main function of road networks is to allow road users reaching their trip destination within a reasonable travel time (TT), the TT of vehicles has been widely used in transport studies as a proxy for network performance (Bhavathrathan and Patil, 2015; Ganin et al., 2017; Omer et al., 2013). The network performance indicator (NP) adopted in this study considers the relative change in TT along the network Origin-Destination (OD) pairs— i.e. combinations of trips' starting and

ending points. The relative changes measured on all OD pairs are then aggregated by a weighting average giving more importance to the OD pairs associated with higher demand.

$$NP = \sum_{w} k_w \Big(1 + \frac{TT_d^w - TT_0^w}{TT_0^w}\Big)^{-1} \tag{1}$$

where w and k_w are an OD pair and the associated weighting factor, respectively; k_w corresponds to the ratio between the demand for w and the total demand in the network; TT_0^w and TT_d^w are the undisrupted and disrupted travel times along w, respectively. NP is scaled in [0,1] and decreases as TT_d^w increases.

This network performance indicator can be complemented by a measure of the unsatisfied demand (USD) that represents the proportion of road users unable to reach their chosen destination in the disrupted network. These users wish to travel between disconnected OD pairs, thus their travel time becomes infinite i.e. $TT_d^w \to \infty$ and $\Big(1 + \frac{TT_d^w - TT_0^w}{TT_0^w}\Big)^{-1} \to 0$.

$$\begin{aligned} &USD = \textstyle\sum_w k_w \delta_w \\ &\text{where } \delta_w = \begin{cases} 0, & \text{if } \Big(1 + \frac{TT_d^w - TT_0^w}{TT_0^w}\Big)^{-1} < 10^{-3} \\ 1, & \text{otherwise} \end{cases} \end{aligned} \tag{2}$$

This set of indicators was developed in Sohouenou et al. (2021), where it is shown that to effectively discriminate between the impacts of scenarios that lead to OD pairs disconnections, it is necessary to consider the impacts on the OD pairs (or road users) separately rather than the often adopted network-wide travel-time losses.

2.2 Recovery process modelling and resilience quantification

2.2.1 Resilience quantification

In this paper, road network resilience is measured by the integral of the road network performance indicator (NP, Eq. 1) over the recovery process (Figure 1). This measure is an adaptation of the seminal framework of Bruneau et al. (2003), where system resilience is measured by the integral over time of the expected degradation in system quality expressed in percentage.

Figure 1 shows the evolution of the road network performance indicator following a multiple-link disruption. The disruption causes a sudden drop in the network performance, which reaches its lowest value at $t = t_0$. Subsequently, the network undergoes a recovery process until $t = t_R$ when the network is fully repaired (the repair could include improvements that lead to a network performance surpassing the original performance if desired). The resilience assessment focuses on the recovery process, which occurs between t_0 and t_H (grey rectangle in Figure 1), where t_H is the time horizon chosen to compute RE, defined here as the maximum time that the recovery process

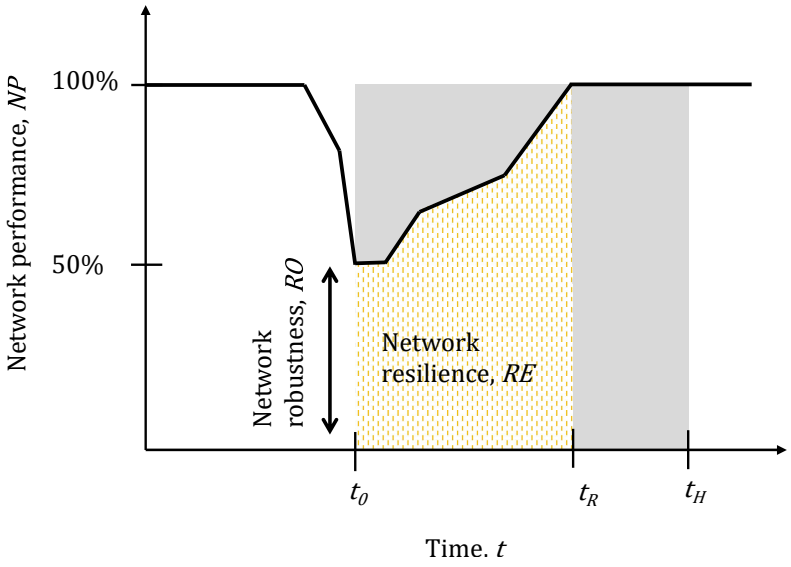

Figure 1: Illustration of the network robustness and resilience concepts and metrics

could require.

The network robustness corresponds to the lowest network performance value reached before the start of the recovery process (Figure 1):

$$RO = NP(t = t_0) \tag{3}$$

The network resilience indicator measures the area below the recovery curve (yellow area in Figure 1). The integral is divided by τ_H to scale RE in [0,1]. This indicator is bounded by a worse-case scenario where the event causes a major decrease in network performance that is not restored until t_H, and a best-case scenario where the event causes a minor decrease in network performance that is rapidly recovered. The network resilience indicator (RE) is defined as follows:

$$RE = \frac{\int_0^{\tau_H} NP(\tau)d\tau}{\tau_H} \tag{4}$$

where $\tau = t - t_0$ is the time elapsed since the incident (or start of the recovery process) at τ_0, and τ_H is the time horizon chosen to compute RE. A fully resilient system would either (i) be very robust i.e. $NP = 100\%$ before any repairs or (ii) be very rapid to recover i.e. NP quickly increases towards 100% as affected links are repaired. In both cases, RE will be close to 100%. On the contrary, a non-resilience network will exhibit a low-performance level slowly increasing with the number of links repaired.

In many works—including in Bruneau et al. (2003) where it was first introduced—system resilience was measured until full recovery (τ_R). However, this expression can provide the same value of resilience for different recovery curves, $NP(\tau)$, (Sharma et al., 2018; Zobel, 2011). In this

work, a fixed time horizon is used to overcome this limitation.

2.2.2 Recovery process model

As explained above, the present paper focuses on link repair sequences and their impacts on the network performance. Hence, recovery progress is measured by the number of links repaired (or cleared) following the disruption rather than the duration of the repair. Under this assumption, the time horizon corresponds to the maximum number of links that can be repaired between t_0 and t_H (N_H), which is also the number of disrupted links, resulting in:

$$RE = \frac{\sum_0^{N_H} NP(x)}{N_H} \tag{5}$$

where x corresponds to the number of links repaired following the disruption.

To conclude, as RE depends on N_H, the resilience of the network to a hazard is characterised by the tuple (RO, RE, N_H).

2.2.3 Recovery strategies

For each disruption scenario considered (Section 2.1), all possible link repair sequences were modelled, and the associated network performance (NP, Eq. 1) recovery curve and resilience indicator (RE, Eq. 5) computed. These results were used to consider two recovery strategies:

- the resilience-optimal recovery curve, obtained by selecting the repair sequence leading to the highest resilience indicator value.
- the average recovery curve, obtained by averaging the NP values of all curves at each stage of the repair process. This curve represents a basic recovery process where the disrupted links are repaired in random order.

To understand the mechanism behind the link order in the optimal recovery process, two additional processes were considered:

- the link-flow based recovery curve, where the links with the highest traffic flow in the undisrupted network are repaired first
- the link-criticality based recovery curve, where the links with the highest criticality value are repaired first. The link criticality measures the impact of the link unavailability on the network performance.

The criticality-based recovery strategy is inspired by criticality studies seeking to identify the links whose failure would result in the highest impacts on the network performance. To identify

critical links in a network, Taylor et al. (2006) proposed an approach based on single-link failures where each link is removed from the network and the corresponding effect on the network performance estimated. The levels of impact are then ranked and the links demonstrating the most significant impacts considered the most critical. This approach has been widely adopted and improved in subsequent studies that also considered link capacity reductions rather than complete link removal (Omer et al., 2013; Sullivan et al., 2010) and multiple-link failures (Sohouenou et al., 2021; Wang et al., 2016).

2.3 Case study

2.3.1 The Sioux Falls network

The present study analyses the resilience of the Sioux Falls (USA) network. Firstly introduced in LeBlanc et al. (1975), the Sioux Falls network (Figure 2) has been extensively used as a case study in the transport literature (Bhavathrathan and Patil, 2015, 2018; Mitradjieva and Lindberg, 2013; Wang et al., 2016). This network consists of 24 nodes, 76 directed links, and 24 OD zones. The datasets describing this case study were obtained from the Transportation Networks for Research repository (Transportation Networks for Research Core Team, 2019). These datasets provide the network structure, link characteristics (including capacity, length and free-flow travel time), and origin-destination trip matrices.

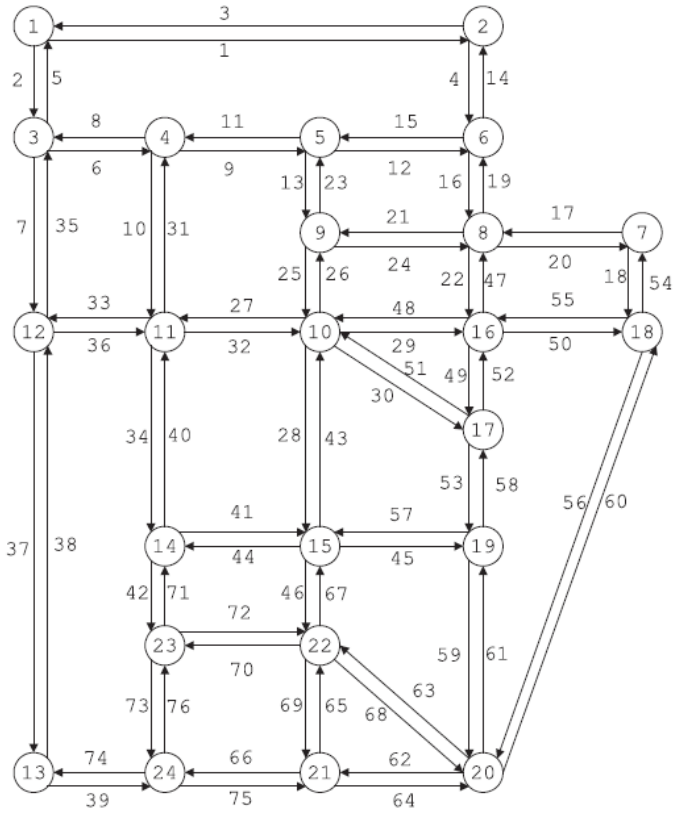

Figure 2: Sioux Falls test network

2.3.2 Transport model

A standard transport model was used to compute and compare the travel time of road users in the initial and disrupted conditions. Using the demand matrix available at the Transportation Networks for Research repository (Transportation Networks for Research Core Team, 2019), traffic was assigned to the network assuming that users independently minimised their travel time. Although individual driving habits may vary (D'Lima and Medda, 2015), this assumption is reasonable in the absence of more detailed data as it has been validated against traffic data from 40 US urban areas (Ganin et al., 2017). This model is the fourth stage of the seminal four-step (trip generation, trip distribution, modal split and traffic assignment) transport model (Ortúzar and Willusem, 2011) that can be used to estimate the number of vehicles (or people) that will use a specific transport facility based on travel data that can be obtained through census information, surveys and estimates.

The travel time of link a (tt_a) is defined by the standard BPR function (Bureau of Public Roads, 1964):

$$tt_a(x_a) = tt_a^f\Big[1 + 0.15\Big(\frac{x_a}{c_a}\Big)^4\Big] \tag{6}$$

where x_a, c_a and tt_a^f are the link flow, capacity and free-flow travel time, respectively.

The simulations were performed in Julia language (v.1.4) using the packages *LightGraphs* and *TrafficAssignement* for network analysis and traffic assignment computation, respectively. The latter implements three methods to find the user equilibrium: the original, conjugate, and bi-conjugate Frank-Wolfe (FW) algorithms (Mitradjieva and Lindberg, 2013). FW algorithm is one of the most popular methods used to solve traffic assignment problems while the conjugate and bi-conjugate versions of this algorithm improve its convergence speed. The fast bi-conjugate FW algorithm was used here with a relative convergence gap of 10^{-4}, which is a sufficient criterion for equilibrium stability (Boyce et al., 2004). To model link closures, a very high free-flow travel time (10,000 min) was assigned to unavailable links.

The transport model implies that the network performance is compared across different equilibrium states, where road users have perfect information of the network state and accordingly minimises their TT. The assumption allows for a fair comparison of the impacts of the link disruptions and repairs on the network performance as the traffic should tend towards these equilibriums following each disruption and repair. However, it is noted that, in reality, the network will go through transition phases as users get updated about the network state and adapt as discussed in Nogal and Honfi (2019).

2.4 Numerical simulations

The links of the Sioux Falls network (Figure 2) were simultaneously disrupted in both directions leading to 38 single- (SLFs), 703 two- (2LFs), 8436 three- (3LFs), and 73,815 four- (4LFs) link failures. Hence, the network performance indicator measured the impact caused by the unavailability of both directions. For consistency, the link flows refer to the sum of the flows in both directions in this paper. However, as the demand in the Sioux Falls network is not totally symmetric a link might be more critical in one direction than the other. Besides, subsets of the 2LF, 3LF, and 4LF scenario sets were considered to assess the difference between the impacts of localised, targeted, and random damage using the disruption model described in Section 2.1.1.

To speed up the resilience analysis, the recovery curves were computed based on the disruption-simulation data as the latter also correspond to the recovery states. For example, the link-repair sequence $[a, b, c]$ leads to the following states: concurrent failure of a, b and c; concurrent failure of b and c; and failure of c; that were all simulated as part of the disruption simulations. Therefore, the numerical simulations were divided into two main parts: the disruption simulations, and the recovery simulations that re-used the disruption data. The disruption and recovery simulations took six hours and five hours 38 min, respectively, using parallel processing on a standard *Intel i3-7100* 3.9GHz and 8GB memory workstation.

Subsets of the 2LF, 3LF, and 4LF scenario sets were considered to assess the difference between the impacts of localised, targeted, and random damage using the disruption model described in Section 2.1.1.

3 Results

3.1 Variations in network resilience due to the recovery strategy

This subsection seeks to evaluate the variations in network resilience due to the recovery strategy to better understand its importance for disruptive event management. To this end, the relationships between the robustness (RO, Eq. 3), unsatisfied demand (USD, Eq. 2) and resilience (RE, Eq. 5) indicators are evaluated across multiple disruption scenarios (Section 3.1.1). The efficiency of the optimal repair strategy (the difference between the resilience indicator values derived from the optimal and average recovery curves) is also evaluated (Section 3.1.2).

3.1.1 Network robustness versus network resilience

Figure 3 shows the relationship between the network robustness and resilience indicators across the damage extension groups in the Sioux Falls network. The resilience indicator values are derived from the average (Figure 3.a) and optimal (Figure 3.b) recovery curves. The results show that the two indicators were linearly correlated for both recovery curves (R^2 between 0.85 ans 0.99) although the strength of the relationship increased with the average recovery curve (Figure 3). This linear relationship implies that when comparing perturbation scenarios that affect the same number of links, the network robustness (or instantaneous performance loss) can explain most of the variations in network resilience. Therefore, the recovery strategy has a minor impact on the network resilience. This impact increases with the damage extension (R^2 decreased as the number of disrupted links increases) and became significant under four-link failures ($R^2 < 0.95$ for both recovery curves).

The unsatisfied demand level is also included in Figure 3, where it seems that USD could also play a role in the prediction model. However, this role was not significant as the double regression performed on the data improved R^2 by around 0.5% only.

Figure 4 shows the relationship between the network robustness and resilience indicators for the three damage types. The linear relationship found between the two metrics across the damage extension groups (Figure 3) remained relevant for the damage types (Figure 4). The strength of the linear model remained high for random and localised disruptions ($R^2 > 0.85$ for both the average and optimal recovery curves) but became moderate under targeted disruptions ($R^2 = 0.79$ and $R^2 = 0.48$ for the average and optimal recovery curves, respectively).

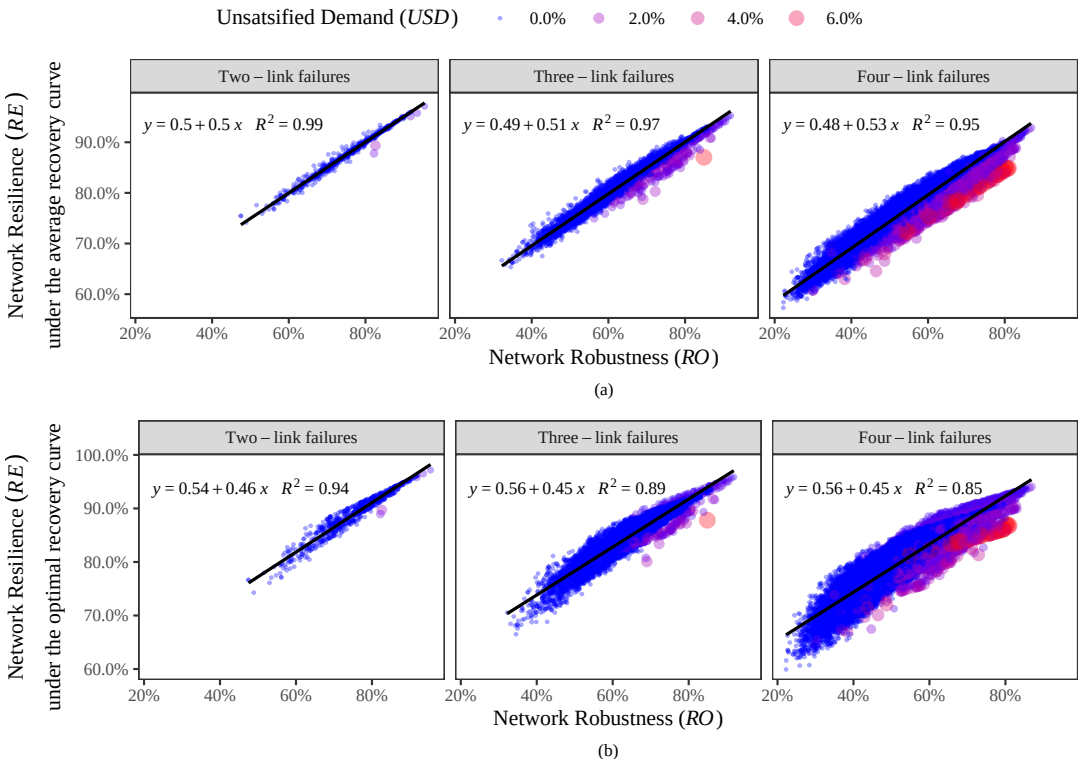

Figure 3: Relationship between the network robustness and resilience indicators across all possible two- to four-link failures in the Sioux Falls, network-resilience computed under the a) average and b) optimal recovery strategies

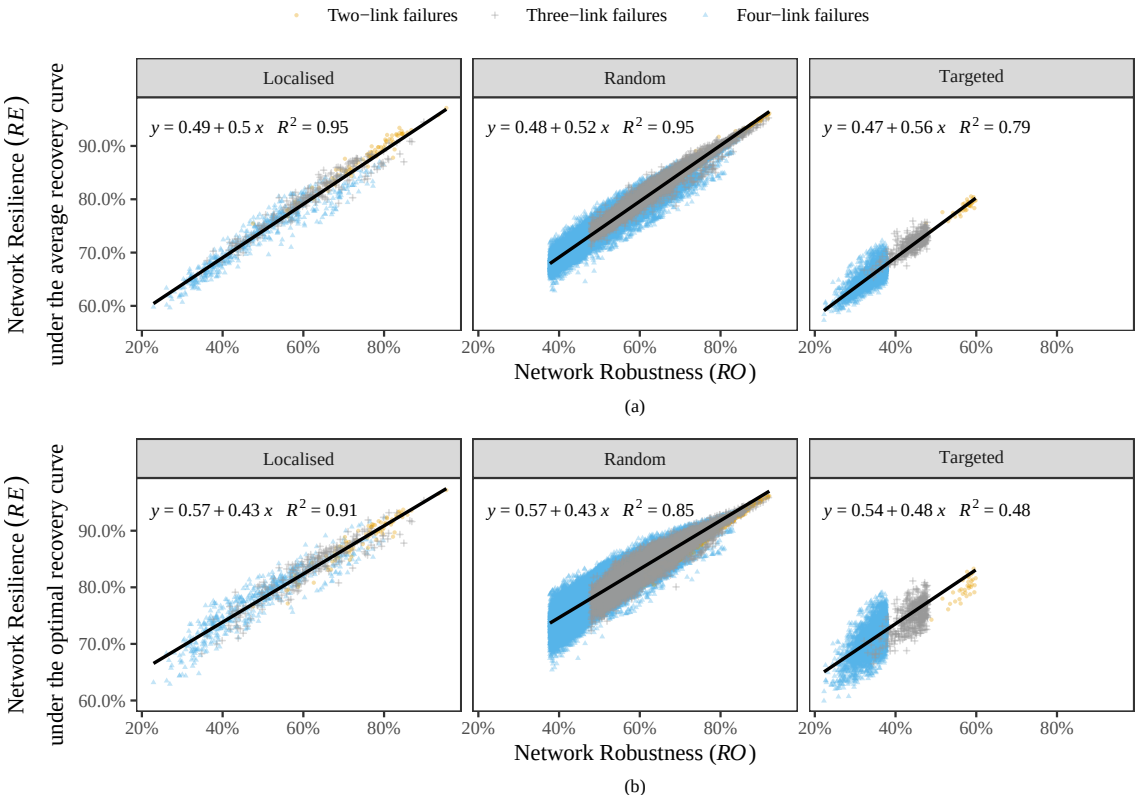

Figure 4: Relationship between the network robustness and resilience indicators across all possible localised-, random- and targeted-link failures concurrently disrupting two- to four- links in the Sioux Falls, network-resilience computed under the a) average and b) optimal recovery strategies

3.1.2 Efficiency of the optimal repair strategy across the disruption scenarios

Figure 5 shows the evolution of the efficiency of the optimal recovery (the difference between the resilience indicator values derived from the optimal and average recovery curves) across the damage extension groups. This Figure shows that the efficiency of the resilience-optimal repair strategy generally increased with the damage extension (as the mean values of the efficiency in the 2LFs, 3LFs and 4LFs were 1.3%, 2.8% and 4.3%, respectively). In addition, the efficiency of the optimal repair strategy was generally higher under targeted attacks than under localised and random link-failures as shown by the positions of the medians in Figure 5. However, the scenarios with the highest efficiency were random failures for all damage extension groups as shown in Figure 5.

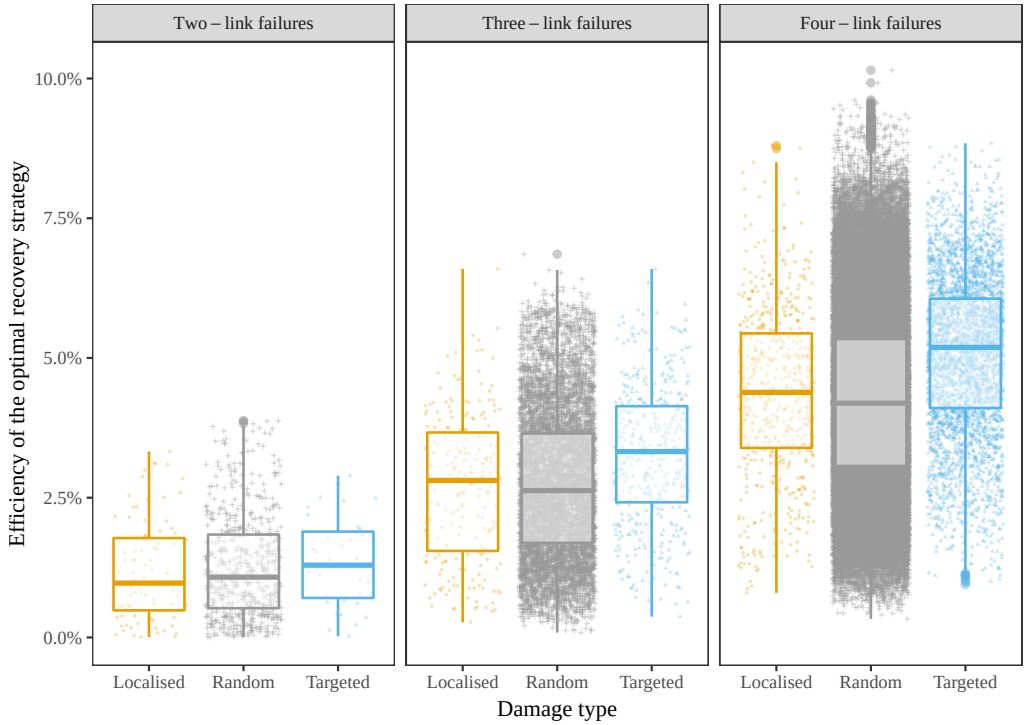

Figure 5: Efficiency of the optimal recovery strategy—i.e. difference between the resilience indicator (RE) value derived from the optimal and average recovery—across the damage extension and type groups

3.2 Identification of the optimal repair strategy

This subsection seeks to characterise the optimal link-order repair strategy and understand the decision-making process that leads to this strategy. To this end, all possible repair strategies are firstly compared under a specific four-link failure scenario for illustrative purposes (Section 3.2.1). This comparison allows the identification of the resilience optimal repair strategy, which is then compared to the criticality- and flow-based repair strategies in this specific scenario (Section 3.2.2). The optimal, flow-based and criticality-based recovery strategies are subsequently compared across

all possible disruption scenarios (Section 3.2.3).

3.2.1 Comparison of all repair strategies following a four-link failure

This sub-subsection focuses on a specific four-link failure scenario where (1,2), (1,3), (10,11) and (10,17) are concurrently disrupted in the Sioux Falls network (Figure 2). This scenario leads to a significant decrease in network performance (NP=66.6%) and a very small proportion of road users unable to reach their chosen destination ($USD = 0.5\%$). The latter is due to the concurrent disruption of (1,2) and (1,3) that isolates node 1 from the rest of the network and disconnects all OD pairs involving this node (as suggested by the network structure shown in Figure 1). Figure 6.a and b show the evolution of the network performance and unsatisfied demand indicators along all possible repair strategies following this disruption scenario, respectively. The recovery curves are represented as step functions because it is assumed that the network performance increased once the links are fully repaired and traffic allowed to use them. The resilience indicator values associated with these different repair strategies are shown in Figure 6 (colour and width of the curves).

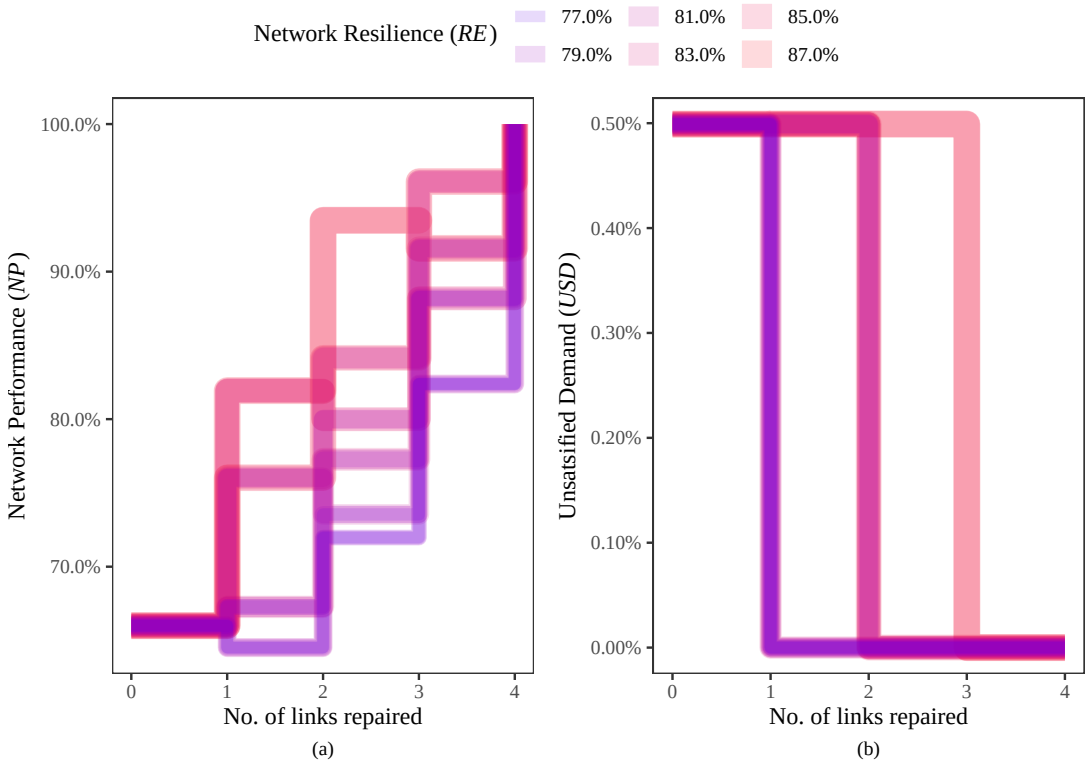

Figure 6: Evolution of the Sioux Falls a) network-performance and b) unsatisfied-demand indicators along all possible recovery processes following the concurrent failure of (1,2), (1,3), (10,11) and (10,17)

It can be observed in Figure 6.a, that the different repair strategies led to a variety of network performance recovery curves. The optimal repair strategy (large and coral-coloured curve) presents

the sharpest increases in NP in the early stage recovery (when the first and second link are repaired), while the repair trajectories associated to the lowest RE values (thin blue curves) present slight network performance increases in the early stage recovery.

Furthermore, some recovery trajectories include a stage when NP slightly drops before increasing to a higher level. For example, the lowest blue curve in Figure 6.a presents a drop in NP following the repair of the first link. The link-repair order that leads to this NP curve is the following: (1,2), (10,11), (10,17) and (1,3). Along this curve, the network performance evolves from $NP = 66.0\%$ ($USD = 0.5\%$) to $NP = 64.5\%$ ($USD = 0\%$), before and after repairing (1,2), respectively. Hence, before (1,2) is repaired 0.5% of vehicles cannot reach their chosen destination. After the repair, these users re-enter the network while there is no increase in capacity, which contributes to a congestion increase that affects the travel time of most travellers such that the overall network performance decreases (from 66.0% to 64.5%). This explanation is confirmed by the evolution of the mean link flow/capacity ratio computed over all links except (1,2) that evolve from 1.65 (sd = 0.73) to 1.70 (sd = 0.78) before and after the repair of (1,2), respectively. This high mean flow/capacity ratio shows that the concurrent unavailability of (1,2), (1,3), (10,11), and (10,17) leads to a highly congested network which is further put under pressure when (1,2) re-opens. Therefore, in this example, it is more efficient to prioritise the re-opening of the inner links (10,11) and (10,17) to reduce the network congestion level before re-opening the outer links (1,2) and (1,3), which allow the users unable to leave/reach node 1 to re-enter the network. This conclusion can also be drawn from Figure 6.b, where it is interesting to note that the resilience-optimal strategy is not optimal in terms of the unsatisfied demand as the USD curve associated to the highest RE values drops after repairing three links.

3.2.2 Comparison between the optimal, criticality-based and flow-based repair strategies

To better characterise the decision-making process that leads to the optimal link repair strategy following the concurrent failure of (1,2), (1,3), (10,11) and (10,17), the latter was compared to two strategies that prioritise the links with the highest traffic flow and criticality values, respectively. The repair sequences and resilience indicator values resulting from these different strategies are shown in Table 2, where the resilience value derived from the average recovery curve is included for comparison. Table 2 shows that the flow- and criticality-based recovery strategies led to resilience indicator values superior to that of the average recovery curve. The criticality-based strategy led to the optimal repair sequence ($RE = 87.5\%$), while the flow-based strategy led to a slightly less efficient repair order ($RE = 85.6\%$), where (1,3) is repaired before (10,17).

Table 2: Comparison of different recovery strategies following the concurrent failure of link (1,2), (1,3), (10,11) and (10,17)

	Optimal recovery	Link-flow based recovery	Link-criticality based recovery	Average recovery curve (1)
Repair sequence	(10,11) (10,17) (1,3) (1,2)	(10,11) (1,3) (10,17) (1,2)	(10,11) (10,17) (1,3) (1,2)	-
Network resilience (RE)	0.875	0.856	0.875	0.816

(1) computed over all possible recovery curves

3.2.3 Comparison of the optimal, criticality-based and flow-based recovery strategies across multiple disruption scenarios

To validate the results obtained in the example above, the resilience indicator values resulting from the criticality- and flow-based repair strategies were compared to that of the optimal and average recovery curves in all two- to four-link-failure scenarios. Figure 7.a and b compare the link flow-based recovery strategy with the average and optimal recovery, respectively. Figure 7.a shows that the flow-based strategy can be more or less efficient than the average recovery depending on the disruption scenario as the dots equally spread above and below the reference line. Figure 7.b shows that the flow-based strategy is rarely optimal as most dots appear below and far from the reference line. Figure 7.c and d compare the link-criticality based recovery strategy with the average and optimal recovery, respectively. Contrary to the flow-based recovery strategy, the criticality-based strategy (Figure 7.c) was more efficient than the average recovery curve in almost all cases as the dots appear above and far from the reference line. Accordingly, the criticality-based strategy was generally optimal or close to optimal as the dots appear close to the reference line in Figure 7.d.

In Figure 7, the damage extension groups are distinguished by different colours and shapes. A visual analysis of these colours and shapes shows that the difference between the network resilience values derived from the different strategies increased with the number of failed links (as 4LF and 3LF scenarios spread further away from the reference line than 3LF and 2LF scenarios, respectively). As the criticality-based recovery is closer to the optimal recovery than the flow-based and average recovery curves (Figure 7), the difference between the criticality and optimal recovery was further investigated. Table 3 shows the evolution of the difference between the resilience indicator values resulting from the optimal and criticality-based recovery strategies across the damage extension groups. This table shows that the mean of the difference between the RE values of the two strategies remained small and slowly increased (from 0% in two- and three-link failures to 0.25% in four-link failures). The maximum value of this difference also increased with the damage extension reaching small but significant values of 4.91% and 6.96% in 3LFs and 4LFs, respectively.

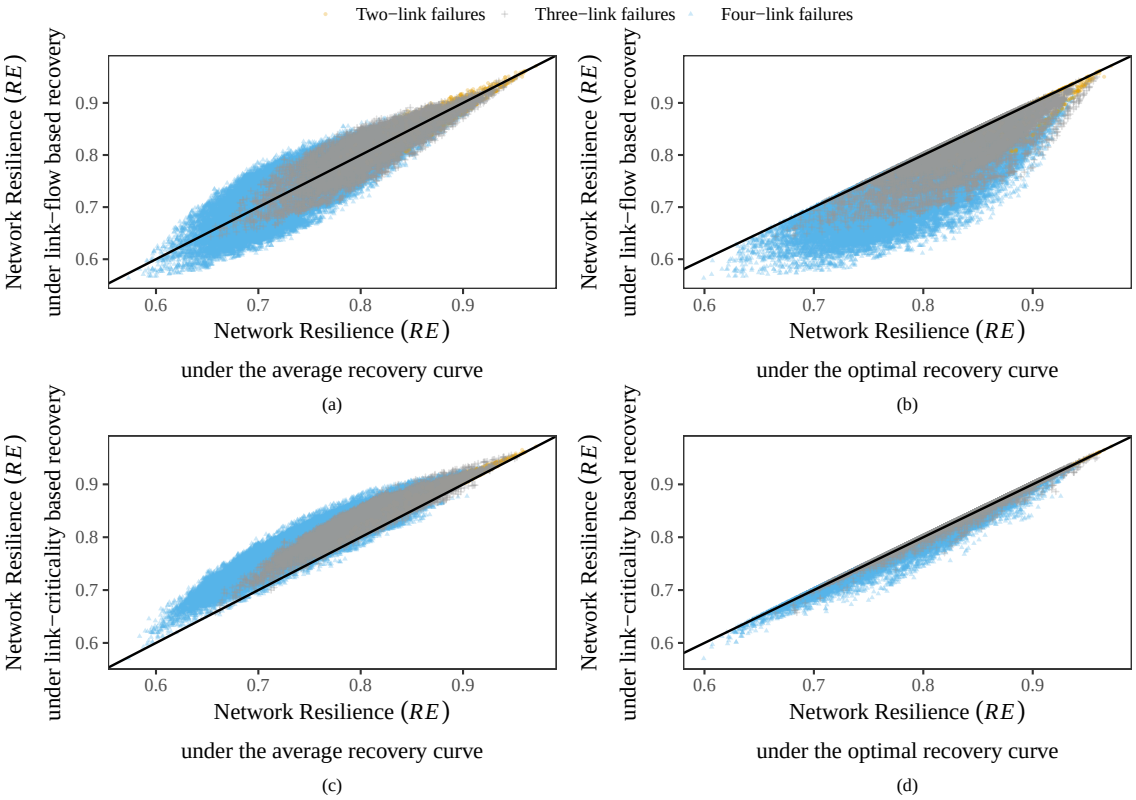

Figure 7: Comparison of the resilience indicator values resulting from different recovery strategies for all possible two- to four-link failures in the Sioux Falls network: a) link-flow based recovery vs average recovery, b) link-flow based recovery vs optimal recovery, c) link-criticality based recovery vs average recovery, d) link-criticality based recovery vs optimal recovery

Table 3: Summary statistics of the difference between the resilience indicator (RE) values resulting from the optimal and link-criticality based recovery strategies across the damage extension groups

	Two-link failures	Three-link failures	Four-link failures
Mean	0.00%	0.00%	0.25%
Standard deviation	0.00%	0.34%	0.61%
Max	0.00%	4.91%	6.96%

4 Discussion

4.1 Importance and role of recovery strategies in network resilience

The comparison of the network robustness and resilience indicators (Figure 3 and 4) showed that although the resilience indicator accounts for the network performance recovery in addition to the instantaneous performance losses (measured by the robustness indicator), the two indicators displayed a very strong linear relationship. This relationship shows that the network robustness bears most of the information about the impact of disruptions. In other words, recovery processes play a minor role in the comparison of the impacts of two damage scenarios such that the scenarios

that lead to the highest instantaneous performance losses tend to also lead to the highest impacts over the recovery process.

Still, the strength of this relationship evolved depending on the recovery strategy considered. For example, in the four-link failures, R^2 went from 0.95 under the average recovery curve to 0.85 under the optimal recovery curve. This suggests that the optimal repair strategy can help counterbalance the instantaneous impact of damage scenarios such that two damage scenarios that lead to similar robustness values (i.e. instantaneous impacts) would lead to different resilience values (i.e. impacts over the recovery process).

Furthermore, the decrease of the strength of the linear model (Figure 3) as the damage extension increases shows that the importance of the role of recovery processes in network resilience gradually increases with the damage extension. Hence, the identification and implementation of the optimal recovery strategy appeared crucial for scenarios disrupting more than four links in the Sioux Falls network. This represents 10% of the links in the Sioux Falls network.

The comparison of the strength of the linear model across the damage types (Figure 4) showed that under random and localised damage the network robustness could explain $\approx$ 95% of the resilience variations with the average recovery curve ($\approx$ 85% with the optimal recovery). This decreased to 79% with the average recovery curve (48% with the optimal recovery) under targeted attacks. This suggested that the identification and implementation of the optimal recovery strategy is crucial for targeted attacks.

Ultimately, the present results show that the network robustness is a good proxy for the network resilience for random and localised scenarios affecting a small number of links. For critical disruption scenarios affecting a large number of links it is important to consider and model recovery processes. The consideration of the latter may, for example, modify the lists identifying the most critical disruption scenarios, used by transport practitioners and public authorises to optimise the allocation of the limited resources available for road infrastructure construction and repair to the most critical scenarios and links.

4.2 Efficiency of the optimal recovery strategy

The evaluation of the efficiency of the optimal recovery strategy—i.e. the difference between the resilience indicator (RE) values derived from the optimal and average recovery—across the different disruption scenarios showed that the optimal repair strategy can lead to significantly higher resilience values (the maximum value of the efficiency was 10.1% for the four-link failures in Figure 5). The analysis of the sensitivity of this efficiency to the damage extension showed that it generally increases with the number of links affected (Figure 5). The mean efficiency values of the optimal recovery went from 1.3% in 2LFs to 2.8% in 3LFs to 4.3% in 4LFs and it can be expected

that these values will continue to increase as the damage extends to more links. The number of possible repair strategies increases with the number of affected links (when R links are affected there are $R!$ possible link-repair sequences) such that the difference between the performance of the optimal and average recovery strategies also increases. Therefore, in accordance with the discussion above, the identification and implementation of the optimal repair strategy become more crucial when several links are affected.

The analysis of the sensitivity of the same efficiency to the damage type led to conflicting results. The efficiency of the optimal recovery strategy appeared generally higher in targeted attacks (as shown by the medians of the boxplots in Figure 5) while the maximum efficiency values did not necessarily appear among targeted attacks (Figure 5). It is hence difficult to characterise the specific scenarios for which the implementation of the optimal recovery strategies would be most effective.

4.3 Optimisation of the recovery strategy at the operational level

The present study also allowed to better characterise the optimal recovery strategy. The analysis of the disruption example (Section 3.2.1) where (1,2), (1,3), (10,11) and (10,17) were concurrently disrupted showed that the optimal repair strategy (maximising the recovery of the network performance indicator) could give priority to the repair of the network inner links that reduce the travel time of most users over the repair of the network-outer links that allow a minority of road users to leave/reach the zones disconnected from the rest of the network. This choice can be explained by the fact that the disruption of the inner links (10,11) and (10,17) lead to severe congestion that would increase further when the minority of stranded users re-enter the network. This would not happen in an uncongested network since the repair of the links allowing stranded road users to leave/reach the zones disconnected from the rest of the network would not affect the travel time of the other users. This shows that it is important to consider and model capacity constraints and congestion, and that the previous studies (Hu et al., 2016; Zhang et al., 2017) that did not consider capacity constraints and potential congestion may incorrectly prioritise the recovery of the network connectivity to the recovery of the users' travel time.

The comparison of the resilience indicator values resulting from the optimal recovery strategy with that of the link-flow and link-criticality based recovery strategies (Section 3.2.2 and 3.2.3) showed that the link criticality-order—based on the impacts of the single-link failures on the network performance—provides relevant information to establish an optimal link repair sequence (Figure 7.c and d), while the link flow provides irrelevant information (Figure 7.a and b). This shows that the identification of an optimal or close to optimal repair strategy requires the computation of disruption scenarios evaluating the impacts of the links unavailability on the network

performance as the metrics based on the network usage in the undisrupted state (such as the link flow) are unable to account for the reserve capacity available in the network to absorb the disruptions.

These results also suggest that the link criticality rankings can be used to find optimal or close to optimal repair strategies with a decreased computational burden. The comparison of all possible repair-orders requires $\sum_{i=1}^{R} \binom{R}{i}$ (15 if $R = 4$) disruption simulations while the identification of the link-criticality based recovery requires R (4 if $R = 4$) disruption simulations, R being the number of disrupted links. Furthermore, considering that the links involved in the most-critical multiple-link failures (MLFs) are not simply the combination of the most-critical links with single-link failure (Wang et al., 2016), it may be possible to increase further the ability of the criticality-based recovery to tend to the optimal-repair strategy by adopting a link criticality indicator based on multiple-link failure simulations such as the one proposed in Sohouenou et al. (2021). The accuracy and extra computational cost of this method will increase with the size of the MLF scenarios considered (i.e. 2LF, 3LF, 4LF, etc.). Future research could seek to determine more precisely when it is necessary to consider 2LF, 3LF, 4LF, etc. and accordingly develop less computationally expensive methods for identifying the optimal recovery strategy.

5 Conclusions

The present paper assessed the effects of link-repair strategies on network resilience and analysed the characteristics of the optimal recovery strategy. Several link-repair strategies were compared across a multitude of perturbation scenarios. This approach allowed the analysis of a large set of scenarios resulting in a clearer understanding of the generality of the results and conclusions. The study led to four main conclusions:

- The network robustness (that measures the initial performance loss of the disrupted network) is a good proxy for the network resilience for random and localised scenarios affecting a small number of links. For critical disruption scenarios affecting a large number of links it is important to consider and model the recovery processes.

- The identification and implementation of the optimal repair strategy become more crucial when several links are affected since this leads to a multitude of decision variables, constraints, and possible alternative strategies.

- It is possible to identify a close to optimal repair strategy with the results of a criticality analysis based on the impact caused by the individual or concurrent failure of the network links.

- The repair strategy should be adapted to the traffic conditions. In uncongested networks (found in rural areas or in off-peak hours in urban areas), the priority should be to reconnect as many people as possible to the network in the early stage recovery. In a highly congested network (found in peak hours in urban areas), it could be beneficial to prioritise the re-opening of the network inner links to reduce the overall congestion before re-opening of the outer links that will reconnect stranded travellers to the network.

The full-scan approach adopted in this study is limited by computational capacity. Although future applications of this approach at larger scales could benefit from an expected growth in computational capacity and an improvement of smarter algorithms, its application is currently realistic for small to medium (sub)network models composed of up to a few hundred links only. The present case study was chosen for computational effectiveness which allowed the performance of an in-depth analysis that resulted in a clearer understanding of road network resilience. Hence, the contribution of this paper lies in the proposed indicators and findings rather than in the full-scan approach, which lacks scalability. These indicators and findings should be of interest to researchers, industry professionals and policy-makers aiming to assess and enhance the resilience of road networks. Future works could extend the present methodology to multimodal transport systems to understand if and how temporary intermodal solutions could be used to optimise congestion and connectivity in early-stage recovery.

Acknowledgements

The research presented in this paper was carried out as part of the H2020-MSCAETN-2016. This project has received funding from the European Union's H2020 Programme for research, technological development and demonstration under grant agreement number 721493.

References

Alcaraz, C. (2018). Cloud-Assisted Dynamic Resilience for Cyber-Physical Control Systems. *IEEE Wireless Communications*, *25*(1), 76–82.

Alcaraz, C., Lopez, J., Rubio, J. E., & Alcaraz, C. (2018). A resilient architecture for the smart grid. *EEE Transactions on Industrial Informatics*, *14*(8), 3745–3753. https://doi.org/10.1109/TII.2018.2826226

Bhavathrathan, B. K., & Patil, G. R. (2015). Quantifying resilience using a unique critical cost on road networks subject to recurring capacity disruptions. *Transportmetrica A: Transport Science*, *11*(9), 836–855. https://doi.org/10.1080/23249935.2015.1087230

Bhavathrathan, B. K., & Patil, G. R. (2018). Algorithm to Compute Urban Road Network Resilience. *Transportation Research Record*, *2672*(48), 104–115. https://doi.org/10.1177/0361198118793329

Boyce, D., Ralevic-Dekic, B., & Bar-Gera, H. (2004). Convergence of traffic assignments: How much is enough? *Journal of Transportation Engineering*, *130*(1), 49–55. https://doi.org/10.1061/(ASCE)0733-947X(2004)130:1(49)

Bruneau, M., Chang, S. E., Eguchi, R. T., Lee, G. C., O'Rourke, T. D., Reinhorn, A. M., Shinozuka, M., Tierney, K., Wallace, W. A., & Von Winterfeldt, D. (2003). A Framework to Quantitatively Assess and Enhance the Seismic Resilience of Communities. *Earthquake Spectra*, *19*(4), 733–752. https://doi.org/10.1193/1.1623497

Bureau of Public Roads. (1964). *Traffic Assignment Manual: Bureau of Public Roads* (tech. rep.). U.S. Department of Commerce. Washington, D.C.

Casali, Y., & Heinimann, H. R. (2019). A topological characterization of flooding impacts on the Zurich road network. *PLoS ONE*, *14*(7). https://doi.org/https://doi.org/10.1371/journal.pone.0220338

Chen, L., & Miller-Hooks, E. (2012). Resilience: An Indicator of Recovery Capability in Intermodal Freight Transport. *Transportation Science*, *46*(1), 109–123. https://doi.org/10.1287/trsc.1110.0376

Demirel, H., Kompil, M., & Nemry, F. (2015). A framework to analyze the vulnerability of European road networks due to Sea-Level Rise (SLR) and sea storm surges. *Transportation Research Part A: Policy and Practice*, *81*, 62–76. https://doi.org/10.1016/j.tra.2015.05.002

D'Lima, M., & Medda, F. (2015). A new measure of resilience: An application to the London Underground. *Transportation Research Part A: Policy and Practice*, *81*, 35–46. https://doi.org/10.1016/j.tra.2015.05.017

Ganin, A. A., Kitsak, M., Marchese, D., Keisler, J. M., Seager, T., & Linkov, I. (2017). Resilience and efficiency in transportation networks. *Science Advances*, *3*(12), e1701079. https://doi.org/10.1126/sciadv.1701079

Gauthier, P., Furno, A., & El Faouzi, N. E. (2018). Road network resilience: how to identify critical links subject to day-to-day disruptions. *Transportation Research Record*, *2672*(1), 54–65. https://doi.org/10.1177/0361198118792115

Hallegatte, S., Rentschler, J., & Rozenberg, J. (2019). *Lifelines: The Resilient Infrastructure Opportunity* (tech. rep.). World Bank. Washington, DC. https://doi.org/10.1596/978-1-4648-1430-3

Henry, D., & Ramirez-Marquez, J. E. (2012). Generic metrics and quantitative approaches for system resilience as a function of time. *Reliability Engineering and System Safety*, *99*, 114–122. https://doi.org/10.1016/j.ress.2011.09.002

Hu, F., Yeung, C. H., Yang, S., Wang, W., & Zeng, A. (2016). Recovery of infrastructure networks after localised attacks. *Scientific Reports*, *6*(24522). https://doi.org/10.1038/srep24522

LeBlanc, L. J., Morlok, E. K., & Pierskalla, W. P. (1975). An efficient approach to solving the road network equilibrium traffic assignment problem. *Transportation Research*, *9*(5), 309–318. https://doi.org/10.1016/0041-1647(75)90030-1

Martinson, R. (2017). Resilience in a Transportation System: A Whole System Approach. *Transportation Research Circular: Transportation Systems Resilience - Preparation, Recovery and Adaptation*, (E-C226), 1–9. http://onlinepubs.trb.org/onlinepubs/circulars/ec226.pdf

Misra, S., Padgett, J. E., Barbosa, A. R., & Webb, B. M. (2020). An expert opinion survey on post-hazard restoration of roadways and bridges: Data and key insights. *Earthquake Spectra*, *36*(2), 983–1004. https://doi.org/10.1177/8755293019891722

Mitoulis, S. A., Argyroudis, S. A., Loli, M., & Imam, B. (2021). Restoration models for quantifying flood resilience of bridges. *Engineering Structures*, *238*(February), (accepted). https://doi.org/10.1016/j.engstruct.2021.112180

Mitradjieva, M., & Lindberg, P. O. (2013). The Stiff Is Moving - Conjugate Direction Frank-Wolfe Methods with Applications to Traffic Assignment. *Transportation Science*, *47*(2), 280–293.

Nogal, M., & Honfi, D. (2019). Assessment of road traffic resilience assuming stochastic user behaviour. *Reliability Engineering and System Safety*, *185*(July 2018), 72–83. https://doi.org/10.1016/j.ress.2018.12.013

Nogal, M., O'Connor, A., Caulfield, B., & Martinez-Pastor, B. (2016). Resilience of traffic networks: From perturbation to recovery via a dynamic restricted equilibrium model. *Reliability Engineering and System Safety*, *156*, 84–96. https://doi.org/10.1016/j.ress.2016.07.020

Omer, M., Mostashari, A., & Nilchiani, R. (2013). Assessing resilience in a regional road-based transportation network. *International Journal of Industrial and Systems Engineering*, *13*(4), 389–408. https://doi.org/10.1504/IJISE.2013.052605

Ortúzar, J. d. D., & Willusem, L. G. (2011). *Modelling Transport* (4th Editio). Oxford, Wiley. https://doi.org/10.1002/9781119993308

Pelling, M., Özerdem, A., & Barakat, S. (2002). The macro-economic impact of disasters. *Progress in Development Studies*, *2*(4), 283–305. https://doi.org/10.1191/1464993402ps042ra

Sharma, N., Tabandeh, A., & Gardoni, P. (2018). Resilience analysis: a mathematical formulation to model resilience of engineering systems. *Sustainable and Resilient Infrastructure*, *3*(2), 49–67. https://doi.org/10.1080/23789689.2017.1345257

Sohouenou, P. Y. R., Neves, L. A. C., Christodoulou, A., Christidis, P., & Lo Presti, D. (2021). Using a hazard-independent approach to understand road-network robustness to multiple disruption scenarios. *Transportation Research Part D: Transport and Environment*. https://doi.org/10.1016/j.trd.2020.102672

Sullivan, J. L., Novak, D. C., Aultman-Hall, L., & Scott, D. M. (2010). Identifying critical road segments and measuring system-wide robustness in transportation networks with isolating links: A link-based capacity-reduction approach. *Transportation Research Part A: Policy and Practice*, *44*(5), 323–336. https://doi.org/10.1016/j.tra.2010.02.003

Taylor, M. A., Sekhar, S. V., & D'Este, G. M. (2006). Application of accessibility based methods for vulnerability analysis of strategic road networks. *Networks and Spatial Economics*, *6*, 267–291. https://doi.org/10.1007/s11067-006-9284-9

Transportation Networks for Research Core Team. (2019). Transportation Networks for Research. Retrieved December 8, 2019, from https://github.com/bstabler/TransportationNetworks

Tuzun Aksu, D., & Ozdamar, L. (2014). A mathematical model for post-disaster road restoration: Enabling accessibility and evacuation. *Transportation Research Part E: Logistics and Transportation Review*, *61*(January), 56–67. https://doi.org/10.1016/j.tre.2013.10.009

Wang, D. Z. W., Liu, H., Szeto, W. Y., & Chow, A. H. F. (2016). Identification of critical combination of vulnerable links in transportation networks – a global optimisation approach. *Transportmetrica A: Transport Science*, *12*(4), 346–365. https://doi.org/10.1080/23249935.2015.1137373

Wisetjindawat, W., Kermanshah, A., Derrible, S., & Fujita, M. (2017). Stochastic Modeling of Road System Performance during Multihazard Events: Flash Floods and Earthquakes. *Journal of Infrastructure Systems*, *23*(4), 04017031. https://doi.org/10.1061/(asce)is.1943-555x.0000391

Xie, F., & Levinson, D. (2011). Evaluating the effects of the I-35W bridge collapse on road-users in the twin cities metropolitan region. *Transportation Planning and Technology*, *34*(7), 691–703. https://doi.org/10.1080/03081060.2011.602850

Zhang, W., Wang, N., & Nicholson, C. (2017). Resilience-based post-disaster recovery strategies for road-bridge networks. *Structure and Infrastructure Engineering*, *13*(11), 1404–1413. https://doi.org/10.1080/15732479.2016.1271813

Zobel, C. W. (2011). Representing perceived tradeoffs in defining disaster resilience. *Decision Support Systems*, *50*(2), 394–403. https://doi.org/10.1016/j.dss.2010.10.001